JOURNAL OF GUIDANCE, CONTROL, AND DYNAMICS
Vol. 27, No. 4, July–August 2004

Solar Sail Attitude Control and Dynamics, Part 1

Bong Wie*
Arizona State University, Tempe, Arizona 85287-6106

Results of a study of developing attitude control systems for solar sail spacecraft are presented. The study objective was to advance sailcraft attitude control technology so that a solar sail spaceflight experiment for validating sail attitude stability, as well as thrust-vector pointing performance, can be conducted in the near future. An overview of sail-attitude-control issues, solar-radiation-pressure models, and dynamic modeling and control analyses of a sailcraft in an Earth-centered elliptic orbit is presented. A simple spin-stabilization approach is emphasized, whereas other active three-axis control approaches, employing a gimbaled control boom, control vanes, or sail shifting/tilting, are presented in the companion paper. A 40 × 40 m, 160-kg sailcraft with a nominal solar-pressure force of 0.01 N, an uncertain center-of-mass/center-of-pressure offset of ±0.1 m (i.e., ±0.25% of 40 m), and moments of inertia of (6000, 3000, 3000) kg · m^2 is used to illustrate the various concepts and principles involved in dynamic modeling and attitude control design.

I. Introduction

A RENEWED interest in solar sailing due to its potential for propellantless space propulsion has spurred recent developments of near-term sail missions and the associated sailcraft technologies.[1–5] The Cosmos-1 solar sail mission of the Planetary Society, with a test flight scheduled for 2004, may become the first experimental solar sailing flight mission in an Earth-centered orbit. The sailcraft development for the Cosmos-1 mission is being conducted in Russia.

Near-term applications of solar sailing technology include high-performance science missions to Mercury, Venus, and the inner solar system. Non-Keplerian orbits, high-velocity missions to the outer planets, and high-velocity interstellar precursor missions (all based on solar sailing technology) are also envisioned by NASA.

A rendezvous mission for Halley's comet studied at the Jet Propulsion Laboratory in 1977 required an 800 × 800 m solar sail for an 850-kg payload/bus as illustrated in Fig. 1 (Ref. 6). However, future solar sail missions will most likely require sails smaller than 100 m due to recent advances in ultralightweight sail films, lightweight deployable booms, and the miniaturization of spacecraft hardware. Detailed historical as well as technical discussions of solar sailing and the associated technologies can be found in Refs. 6–8.

Following Garwin's publication on solar sailing in 1958,[9] attitude stabilization of a space vehicle by solar radiation pressure was first proposed by Sohn in 1959.[10] Since then, the concept of using solar radiation pressure for attitude stabilization as well as stationkeeping control of various satellites has been studied extensively by many researchers during the past three decades.[11–15]

In fact, such a solar-pressure attitude control concept has been successfully implemented on a certain type of geostationary satellites as well as on several interplanetary spacecraft. For example, the large solar-radiation disturbance torque caused by an asymmetrical solar array configuration of INSAT and GOES satellites with only one solar array wing on the south side is countered by a conical-shaped solar sail on a long boom mounted on the north side.

The roll/yaw control systems of geosynchronous communications satellites such as OTS, TELECOM 1, and INMARSAT 2 successfully utilized the solar-pressure attitude control concept. An asymmetrical offset of the solar array wings from their nominal sun-pointing orientation generates so-called windmill torque, as illustrated in Fig. 2a. The nominal sun-pointing orientation of the north and south solar array wings is shown in Fig. 2b. In Fig. 2, the Earth-pointing main body of the spacecraft is not shown. For typical geosynchronous communications satellites, the body-fixed pitch axis is perpendicular to the orbital plane, the roll axis along the flight direction, and the yaw axis toward the Earth. If the north and south solar array wings are not rotated asymmetrically (i.e., $\delta_N \neq -\delta_S$), then an additional roll/yaw torque, perpendicular to the windmill torque, is also generated, as illustrated in Fig. 2c. Additional flaps mounted on the outermost solar panels substantially increase the roll/yaw control torques. Note that such flaps produce windmill torque even when $\delta_N = \delta_S = 0$. The maximum offset of each array is constrained by the acceptable electrical power loss (nominally 1%). Detailed descriptions of such a flight-proven solar-pressure attitude control technique can be found in Refs. 16–19.

The idea of asymmetrically twisting solar panels to create windmill torque about the roll axis was also successfully applied to the Mariner 10 spacecraft during its flight to Mercury. However, its roll attitude control was done by commands from the mission controllers because there was no onboard controller for that task.

Even though the effectiveness of solar-pressure attitude control has been validated in flight as discussed in this section, the solar radiation pressure is often considered as an external disturbance for most satellites. Recently, solar-pressure effects on formation flying of small satellites were investigated in Refs. 20 and 21. The significant effects of solar radiation pressure on attitude and orbit control of very large space solar power satellites (SSPS) in geosynchronous orbit were also recently studied in Ref. 22.

During the past three decades a variety of advanced dynamic modeling and spacecraft control techniques have been developed. Detailed descriptions of such advanced technologies associated with spacecraft dynamics and control problems can be found in Refs. 19, 23, and 24.

However, there exist various practical implementation issues to be resolved in applying these advanced control techniques to active three-axis attitude control of near-term sailcraft as well as to future advanced sailcraft. All practical spacecraft control designs are subject to the physical limits of actuators, sensors, spacecraft structural rigidity, and other mission constraints. In particular, when a gimbaled control boom and/or sail control vanes (instead of conventional thrusters, reaction wheels, and magnetic torquers) are to be employed as primary actuators for active three-axis attitude control of solar sail spacecraft, there exist a variety of practical issues to be resolved. Therefore, solar sail attitude and flight-control technology needs to be rapidly advanced so that a sail spaceflight experiment

Received 3 June 2002; presented as Paper 2002-4573 at the AIAA Guidance, Navigation, and Control Conference, Monterey, CA, 2–6 August 2002; revision received 25 August 2003; accepted for publication 3 November 2003.

*Professor, Department of Mechanical and Aerospace Engineering; bong.wie@asu.edu. Associate Fellow AIAA.

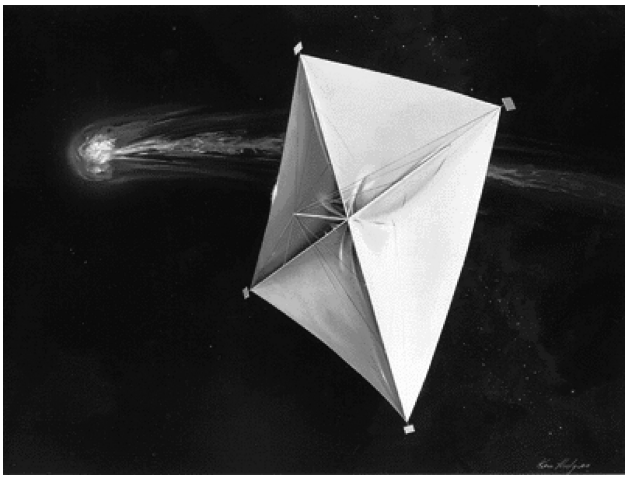

Fig. 1 Large solar sail spacecraft controlled by four control vanes mounted at the spar tips.[6]

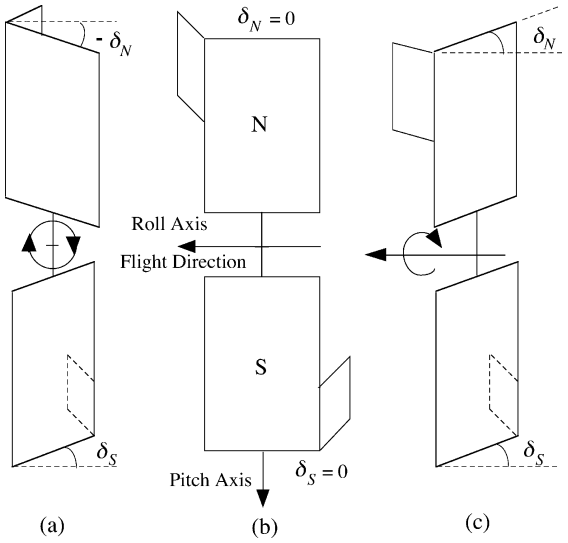

Fig. 2 Illustration of a solar-pressure attitude control concept successfully implemented on geosynchronous communications satellites, such as OTS, TELECOM 1, and INMARSAT 2 (Refs. 16–19).

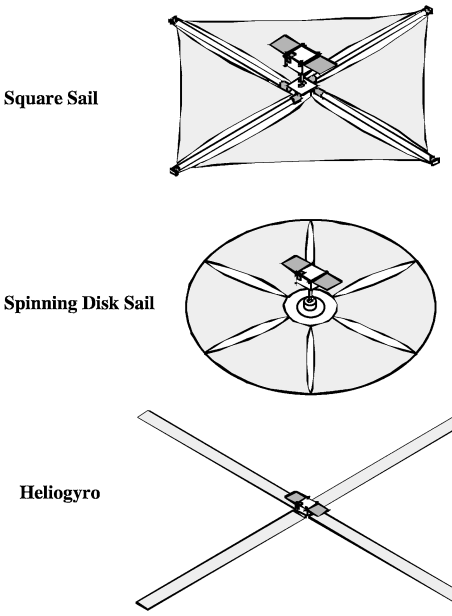

Fig. 3 Three basic types of near-term sailcraft.[1]

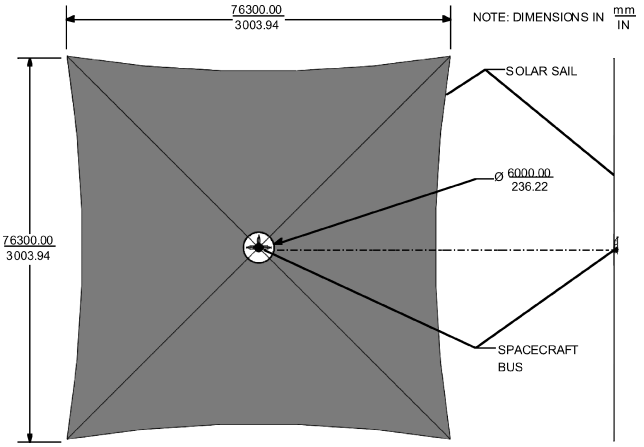

Fig. 4 ST5 Geostorm solar sail.[2]

for validating sail attitude stability and thrust-vector pointing performance can be conducted in the near future.

The remainder of this paper is outlined as follows: In Sec. II, an overview of sail attitude control issues is presented. Section III describes solar-radiation-pressure force modeling for solar sails. Section IV describes a simple spin-stabilization concept for countering the significant effect of a solar pressure disturbance torque, caused by an uncertain cm/cp offset. In Sec. V, dynamic modeling and attitude control of a sailcraft in an Earth-centered elliptic orbit are described.

Detailed dynamic modeling and attitude control design for a sailcraft employing a two-axis gimbaled control boom, control vanes, or translating/tilting sail panels are presented in Part 2 (Ref. 25).

II. Solar Sail Attitude Control Issues

Three basic types of near-term sailcraft are shown in Fig. 3. These configurations have advantages and disadvantages in terms of control authority, controllability, packaging, deployment, and other system-level tradeoff issues (i.e., mass, cost, etc.). Selecting a particular sail configuration for a specific mission is a complex problem, requiring detailed system-level tradeoffs. This paper focuses on a square sail configuration, which is most likely to be chosen for various near-term sail missions (Refs. 1–5).

As discussed in Refs. 10 and 11, an interplanetary spacecraft is often said to be statically stable when its center of mass lies between the sun and its center of pressure. Although any point along the resultant solar-pressure force direction can be considered as the center of pressure, the location along a spacecraft reference line through which the resultant force is acting is often defined as the center of pressure. Whenever a statically stable sailcraft rotates away from its neutral sun-pointing orientation, a restoring (stabilizing) torque is generated. The dynamical behavior of such a statically stable sailcraft is analogous to that of a gravity-gradient-stabilized satellite. That is, if disturbed, the sailcraft will oscillate indefinitely. If the center of pressure lies between the sun and the center of mass, a destabilizing torque is generated whenever the sailcraft rotates away from its null or trim orientation.

A spin-stabilized 76×76 m square sailcraft, shown in Fig. 4, has been proposed for the New Millennium Program Space Technology 5 (ST5) Geostorm warning mission, which would provide real-time monitoring of solar activity.[2] It would operate inside the L_1 point of the sun–Earth system toward the sun and increase the warning time for geomagnetic storms compared to a vantage point closer to the Earth. For such a large sailcraft with moments of inertia of (44,000, 22,000, 24,000) $\text{kg} \cdot \text{m}^2$, an uncertain center-of-mass/center-of-pressure (cm/cp) offset of approximately 1 m was assumed by the Geostorm sail study team and a spin rate of 0.45 deg/s was selected to keep the angular momentum vector within 1 deg of the sunline. Thrusters are used for precession/nutation control as well as spin-rate control of this sailcraft.

A 76 × 76 m sailcraft is currently under development by Team Encounter.[3,4] It is planned to be launched as a secondary payload on an Ariane 5. A combination of passive and active attitude control techniques are employed for this sailcraft. A Team Encounter sailcraft with a total mass of 18 kg is required to achieve solar system escape within 3 or 5 years. Its sun-pointing orientation is passively stabilized. A constant pitch angle of 25 deg with respect to the sun is required during the first 300 days after separation from a carrier spacecraft. The 25-deg pitch trim angle is passively maintained by an intentional cm/cp offset caused by a 3-kg payload tied to the side with a burnwire. The rotational motion about the sun vector is actively controlled. An onboard star camera measures the sailcraft orientation with respect to a fixed star field and the control vanes provide the necessary control torque to counteract a windmill disturbance torque of 0.1 mN-m. After 300 days, an onboard timer will power the burnwire to release the payload restrained by a suspension wire. Consequently, the center of mass will move to the sailcraft center and the sailcraft will be passively stabilized for a zero pitch trim angle. Detailed preliminary design results of the Team Encounter sailcraft can be found in Refs. 3 and 4.

The ST5 Geostorm solar sail, as well as the Team Encounter solar sail, was designed by L'Garde. A square sail with four triangular control vanes, being developed by L'Garde for a NASA In-Space Propulsion solar sail ground demonstration, is illustrated in Fig. 5.

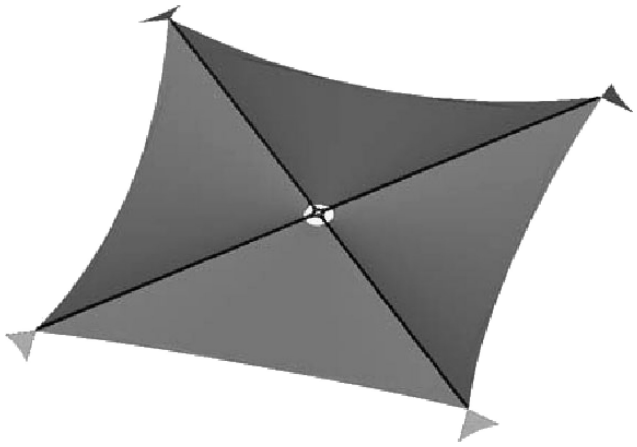

Fig. 5 Square solar sail under development by L'Garde for a NASA in-space propulsion solar sail ground demonstration in 2005.

Although a passive or spin-stabilization technique can be very cost-effective for certain missions, such as the Team Encounter mission or the Geostorm warning mission, active three-axis attitude control will be necessary for most sailcraft, requiring continuous thrust-vector steering maneuvers.

One method of actively controlling the attitude of a three-axis-stabilized sailcraft is to employ small reflective control vanes mounted at the spar tips, as can be seen in Figs. 1 and 5. Another method is to change its center-of-mass location relative to its center-of-pressure location. This can be achieved by articulating a control boom with a tip-mounted payload/bus. Such a concept of articulating a two-axis gimbaled control boom was investigated for a 40 × 40 m square sailcraft (Fig. 6), and it was proposed for the New Millennium program Space Technology 7 (ST7) sail flight validation experiment (Ref. 5).

Similarly to the problem inherent in the various sail configurations, these different attitude-control methods do also have their own advantages and disadvantages in terms of control authority, controllability, and other system-level tradeoff issues.

Although the essential idea behind all these "cm/cp methods" appears simple, there are challenging hardware implementation problems to be solved. Some technical issues inherent in the development of an attitude control subsystem for a square sailcraft are briefly discussed.

Attitude control and stabilization of a sailcraft may also be possible by use of a typical attitude control subsystem, which is often a necessary part of the sailcraft bus. However, small reaction wheels and/or a propulsion subsystem with a limited amount of propellant to be employed for a typical 100-kg bus may be inefficient or ineffective for a fully deployed sailcraft because of its large moments of inertia, its large solar-pressure disturbance torque, and its extended sailing voyages. For example, a 40 × 40 m, 160-kg sailcraft with a nominal solar-pressure force of 0.01 N and a cm/cp offset of ±0.1 m has a solar-pressure disturbance torque of $\pm 0.001\ \mathrm{N \cdot m}$, which is about 100 times larger than that of typical geosynchronous communications satellites. A conventional three-axis attitude control system will require large reaction wheels and also a prohibitively large amount of propellant to counter such a major disturbance torque acting on a sailcraft.

Consequently, the use of a gimbaled control boom, control vanes, sail panel translation/rotation, control-mass translation, or possibly reflectivity modulation is necessary for three-axis attitude control of sailcraft. In addition to these propellantless sail-control actuators, three-axis attitude information is crucial for active three-axis attitude control and thrust-vector pointing/steering. It is assumed

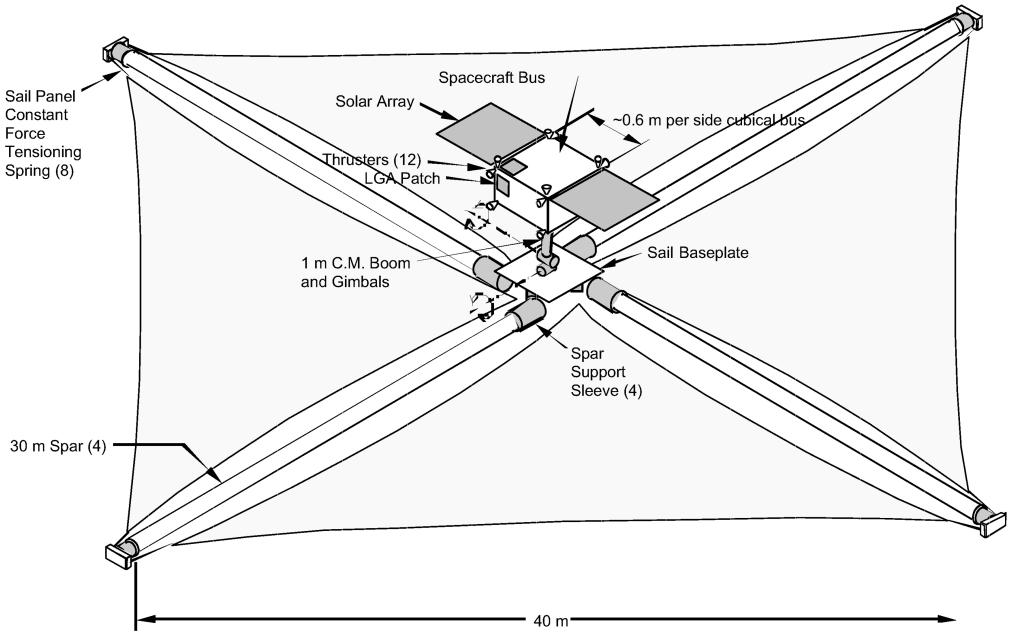

Fig. 6 A 40 × 40 m, 160-kg sailcraft configuration (not to scale), designed by JPL and AEC–Able Engineering for the NMP ST7 sail flight experiment.[1,5]

that three-axis inertial attitude information will be available from an attitude determination subsystem consisting of sun sensors, star cameras, and rate gyros.

One of the critical parameters of sailcraft is the sun angle between the sail-surface normal and the sun, often denoted by α. Its significant effects on the overall performance, stability, and control of a sailcraft are similar to the effects of the aircraft angle of attack, α, on aircraft performance, stability, and control. Similar to the so-called high-α control problem of high-performance aircraft, a high-performance sailcraft may also have a similar high-α control problem because of its thrust-vector pointing requirement of typically $\alpha \approx 35$ deg.

The basic principle behind various aerodynamic control surfaces of aircraft, such as ailerons, elevator, rudder, flaps, trim tabs, and spoilers, should be exploited in developing a sail attitude and flight control subsystem. Furthermore, uncertainties inherent in solar radiation pressure modeling of nonperfect and nonflat sails should be taken into account in designing a sail-attitude-control subsystem.

III. Solar Radiation Pressure Models

In this section, solar-radiation-pressure (SRP) models for the purpose of sail-attitude-control analysis and design are described. These models do not include the effects of sail film wrinkles, thermal deformation, or structural vibration. Throughout this paper, solar sails are assumed to be rigid (although they are in fact large, flexible membrane structures), because attitude control and thrust-vector steering are to be performed very slowly to avoid exciting structural-mode vibrations.

The SRP forces are due to photons impinging on a surface in space. If a fraction ρ_a of the impinging photons are absorbed, a fraction ρ_s are specularly reflected, and a fraction ρ_d are diffusely reflected by a surface, then we have

$$\rho_a + \rho_s + \rho_d = 1 \tag{1}$$

The SRP force acting on such a flat Lambertian surface located 1 astronomical unit (AU) from the sun is modeled as

$$\begin{aligned}\boldsymbol{F} &= PA\left[\rho_a(\boldsymbol{S}\cdot\boldsymbol{n})\boldsymbol{S} + 2\rho_s(\boldsymbol{S}\cdot\boldsymbol{n})^2\boldsymbol{n} + \rho_d(\boldsymbol{S}\cdot\boldsymbol{n})(\boldsymbol{S} + \tfrac{2}{3}\boldsymbol{n})\right] \\ &= PA(\boldsymbol{S}\cdot\boldsymbol{n})\left\{(\rho_a + \rho_d)\boldsymbol{S} + \left[2\rho_s(\boldsymbol{S}\cdot\boldsymbol{n}) + \tfrac{2}{3}\rho_d\right]\boldsymbol{n}\right\} \\ &= PA(\boldsymbol{S}\cdot\boldsymbol{n})\left\{(1 - \rho_s)\boldsymbol{S} + \left[2\rho_s(\boldsymbol{S}\cdot\boldsymbol{n}) + \tfrac{2}{3}\rho_d\right]\boldsymbol{n}\right\}\end{aligned} \tag{2}$$

where $P = 4.563 \times 10^{-6}$ N/m^2 is the nominal solar-radiation-pressure constant 1 AU from the sun, A is the surface area, $\boldsymbol{n}$ is a unit vector normal to the surface, and $\boldsymbol{S}$ is a unit vector pointing from the sun to the surface, as shown in Fig. 7. The solar radiation pressure varies inversely with the square of the distance from the sun. [Note that solar-pressure force equations given in Ref. 26 need to be properly changed to the forms of Eq. (2).]

Because $\boldsymbol{S} = \cos\alpha\boldsymbol{n} + \sin\alpha\boldsymbol{t}$, where α is the sun angle between the surface normal and the sunline and $\boldsymbol{t}$ is the transverse unit vector, as shown in Fig. 7, the SRP force can also be expressed as

$$\boldsymbol{F} = F_n\boldsymbol{n} + F_t\boldsymbol{t} \tag{3}$$

where

$$F_n = PA\left\{(1 + \rho_s)\cos^2\alpha + \tfrac{2}{3}\rho_d\cos\alpha\right\}$$

$$F_t = PA(1 - \rho_s)\cos\alpha\sin\alpha$$

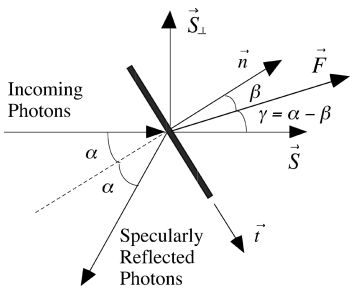

Fig. 7 Solar-radiation-pressure force model of a nonperfect flat surface.

For a case with $\rho_d \approx 0$, we may also express the SRP force as

$$\begin{aligned}\boldsymbol{F} &= PA\cos\alpha\{(1 - \rho_s)\boldsymbol{S} + 2\rho_s\cos\alpha\boldsymbol{n}\} \\ &= PA\cos\alpha\{(1 - \rho_s)\boldsymbol{S} + 2\rho_s\cos\alpha(\cos\alpha\boldsymbol{S} + \sin\alpha\boldsymbol{S}_\perp)\} \\ &= PA\cos\alpha\{(1 - \rho_s + 2\rho_s\cos^2\alpha)\boldsymbol{S} + 2\rho_s\cos\alpha\sin\alpha\boldsymbol{S}_\perp\} \\ &= PA\cos\alpha\{(1 + \rho_s\cos 2\alpha)\boldsymbol{S} + \rho_s\sin 2\alpha\boldsymbol{S}_\perp\} \\ &= F_s\boldsymbol{S} + F_\perp\boldsymbol{S}_\perp\end{aligned} \tag{4}$$

where $\boldsymbol{S}_\perp$ is a unit vector perpendicular to $\boldsymbol{S}$ and is in the same plane as $\boldsymbol{S}$ and $\boldsymbol{n}$.

For sails in sun-centered orbits, the components along the sunline and perpendicular to the sunline are sometimes called the "drag" and "lift" components, respectively. The transverse component, $F_\perp$, provides effective thrust control for orbital maneuvering of sailcraft in sun-centered orbits. For example, the sun angle that maximizes the transverse component can be found as

$$\frac{\mathrm{d}}{\mathrm{d}\alpha}F_\perp = 0 \Longrightarrow \frac{\mathrm{d}}{\mathrm{d}\alpha}\cos^2\alpha\sin\alpha = 0 \tag{5}$$

which gives $\alpha = \tan^{-1}(1/\sqrt{2}) = 35.26$ deg. This optimal sun angle of 35.26 deg for maximizing the transverse component is often selected as the desired pitch orientation of an interplanetary sailcraft in a sun-centered orbit.

The normal and transverse components of the SRP force acting on a flat sail surface with its more detailed optical and thermal properties are also described in Chapter 2 of Ref. 8 and Appendix A of Ref. 6:

$$\frac{F_n}{PA} = (1 + rs)\cos^2\alpha + B_f r(1 - s)\cos\alpha + \frac{e_f B_f - e_b B_b}{e_f + e_b}(1 - r)\cos\alpha \tag{6}$$

$$\frac{F_t}{PA} = (1 - rs)\cos\alpha\sin\alpha \tag{7}$$

$$F = \sqrt{F_n^2 + F_t^2} \tag{8}$$

$$\tan\beta = \frac{F_t}{F_n} \tag{9}$$

B_f, B_b = non-Lambertian coefficients for front and back surfaces, e_f, e_b = front and back surface emission coefficients, r = reflectivity of front surface, s = specular reflection coefficient, and β = angle of SRP force vector from surface normal.

For a square sailcraft similar to the one illustrated in Fig. 1, we have the following optical properties (Appendix A of Ref. 6):

$$\begin{aligned} B_f &= 0.79, & B_b &= 0.55 \\ e_f &= 0.05, & e_b &= 0.55 \\ r &= 0.88, & s &= 0.94 \end{aligned}$$

The resulting normal and transverse components of the SRP force become

$$\begin{aligned}F_n/PA &= 1.8272\cos^2\alpha + 0.0417\cos\alpha - 0.0526\cos\alpha \\ &= 1.8272\cos^2\alpha - 0.0109\cos\alpha\end{aligned} \tag{10a}$$

$$F_t/PA = 0.1728\cos\alpha\sin\alpha \tag{10b}$$

In practice, the pressure distribution is not uniform across the surface of a sail due to curvature (billow). A numerical integration of the F_n and F_t equations across the curved surface of the sail is needed to determine the resulting pressure distribution. This requires an iterative process since the pressure distribution is a function of the sail shape, and vice versa the shape is a function of the pressure distribution. For the sailcraft shown in Fig. 1, such an iterative process was used by JPL to find a parameterized model of the form (Appendix B of Ref. 6)

$$F = \eta PA(0.349 + 0.662\cos 2\gamma - 0.011\cos 4\gamma) \tag{11}$$

where $\eta = 1.816$ and $\gamma = \alpha - \beta$.

The SRP force acting on a sail surface with area A is also often approximated as

$$F \approx \eta P A \cos^2\alpha \tag{12}$$

where η is called the overall sail thrust coefficient, typically around 1.8 for a real sailcraft with sail wrinkles and billowing, with an ideal maximum value of $\eta_{\max} = 2$.

IV. Spin Stabilization of Sailcraft

A simple solution to the problem of maintaining a desired orientation of a sailcraft in the presence of a cm/cp offset is to spin the sailcraft. A thrust-vector misalignment with the center of mass will cause the sailcraft to tumble in the absence of spinning or active three-axis control. However, a spinning sailcraft possesses a gyroscopic stiffness to external disturbances, and its motion under the influence of external disturbances is characterized by the precession and nutation of the spin axis. The orientation of a spinning sailcraft can be changed by precession of the sailcraft using thrusters. Tilting and/or translating sail panels can also provide an effective precession control torque to a spinning sailcraft with a large angular momentum.

For example, a spin-stabilization approach was chosen for a 76×76 m square sailcraft of the NMP ST5 Geostorm warning mission.[2] For such a large sailcraft with moments of inertia of (44,000, 22,000, 24,000) kg $\cdot$ m^2, an uncertain cm/cp offset of approximately 1 m was assumed by the Geostorm sail study team and a spin rate of 0.45 deg/s was then selected to keep the angular momentum vector within 1 deg of the sunline.

In this section, an analytic approach often employed for the dynamic analysis of a spinning body with thrust-vector misalignment, as discussed in Ref. 24 (pp. 352–355), is applied to a spinning solar sail with a cm/cp offset.

A. Spinning Sailcraft with a CM/CP Offset

Consider a sailcraft possessing a body-fixed reference frame B with basis vectors $\{\boldsymbol{b}_1, \boldsymbol{b}_2, \boldsymbol{b}_3\}$ and with its origin at the center of mass. The reference frame B coincides with principal axes. It is assumed that the first axis is the roll (spin) axis perpendicular to the sail surface and the second and third axes are the pitch/yaw (transverse) axes. The solar-pressure force vector is nominally aligned along $\boldsymbol{b}_1$ through the center of pressure of the sailcraft.

Euler's rotational equations of motion for a rigid sailcraft are simply given by

$$J_1\dot{\omega}_1 - (J_2 - J_3)\omega_2\omega_3 = T_1 \tag{13a}$$

$$J_2\dot{\omega}_2 - (J_3 - J_1)\omega_3\omega_1 = T_2 \tag{13b}$$

$$J_3\dot{\omega}_3 - (J_1 - J_2)\omega_1\omega_2 = T_3 \tag{13c}$$

where $\omega_i \equiv \boldsymbol{b}_i \cdot \boldsymbol{\omega}$ are the body-axis components of the angular velocity of the sailcraft and T_i are the external-torque-vector components along the body axes.

For a square (or an axisymmetric circular) sailcraft with $J_2 = J_3 = J$, the rotational equations of motion become

$$J_1\dot{\omega}_1 = 0 \tag{14a}$$

$$J\dot{\omega}_2 - (J - J_1)\omega_3\omega_1 = T_2 \tag{14b}$$

$$J\dot{\omega}_3 - (J_1 - J)\omega_1\omega_2 = T_3 \tag{14c}$$

where T_2 and T_3 are the solar-pressure-torque-vector components caused by a cm/cp offset. The windmill torque about the spin (roll) axis is ignored here; i.e., it is assumed that $T_1 \approx 0$.

From Eq. (14a), we have

$$\omega_1 = \text{constant} = \Omega \tag{15}$$

where the constant Ω is called the *spin rate* of the sailcraft about its roll axis $\boldsymbol{b}_1$. For simplicity, it is assumed that the pitch/yaw transverse axes are chosen so that $T_2 = 0$ and $T_3 = \epsilon F$, where ϵ is a cm/cp offset distance and F is the solar-pressure force. It is further assumed that the solar-pressure force is nearly constant regardless of coning motion of the roll axis, although it is a function of the spin-axis orientation relative to the sun.

Equations (14b) and (14c) then become

$$\dot{\omega}_2 = -\lambda\omega_3 \tag{16a}$$

$$\dot{\omega}_3 = \lambda\omega_2 + a \tag{16b}$$

where $\lambda = \Omega(J_1 - J)/J$ and $a \equiv \epsilon F/J$ denotes the disturbance acceleration resulting from a cm/cp offset. Note that a is assumed to be constant.

To describe the rotational motion of the spinning sailcraft as seen from an inertial reference frame, we consider the roll $\leftarrow$ pitch $\leftarrow$ yaw rotational sequence: $\boldsymbol{C}_1(\theta_1) \leftarrow \boldsymbol{C}_2(\theta_2) \leftarrow \boldsymbol{C}_3(\theta_3)$. For this rotational sequence, we have the following kinematic differential equations:

$$\dot{\theta}_1 = \omega_1 + (\omega_2 \sin\theta_1 + \omega_3 \cos\theta_1)\tan\theta_2 \tag{17a}$$

$$\dot{\theta}_2 = \omega_2 \cos\theta_1 - \omega_3 \sin\theta_1 \tag{17b}$$

$$\dot{\theta}_3 = (\omega_2 \sin\theta_1 + \omega_3 \cos\theta_1)/\cos\theta_2 \tag{17c}$$

For small θ_2, these kinematic differential equations become

$$\dot{\theta}_1 = \omega_1 + \dot{\theta}_3\theta_2 \tag{18a}$$

$$\dot{\theta}_2 = \omega_2 \cos\theta_1 - \omega_3 \sin\theta_1 \tag{18b}$$

$$\dot{\theta}_3 = \omega_2 \sin\theta_1 + \omega_3 \cos\theta_1 \tag{18c}$$

Assuming $\theta_2\dot{\theta}_3 \ll \omega_1$, we can further approximate $\dot{\theta}_1$ as

$$\dot{\theta}_1 \approx \omega_1 = \Omega = \text{constant} \tag{19}$$

and $\theta_1 \approx \Omega t$.

Finally, we obtain a set of linearized equations of motion as follows:

$$\dot{\omega}_2 = -\lambda\omega_3 \tag{20a}$$

$$\dot{\omega}_3 = \lambda\omega_2 + a \tag{20b}$$

$$\dot{\theta}_2 = \omega_2 \cos\Omega t - \omega_3 \sin\Omega t \tag{20c}$$

$$\dot{\theta}_3 = \omega_2 \sin\Omega t + \omega_3 \cos\Omega t \tag{20d}$$

The solutions of Eqs. (20a) and (20b) for a constant disturbance acceleration a can be found as

$$\omega_2(t) = \omega_2(0)\sin\lambda t - \omega_3(0)\cos\lambda t - (a/\lambda)(1 - \cos\lambda t)$$

$$\omega_3(t) = -\omega_2(0)\cos\lambda t - \omega_3(0)\sin\lambda t + (a/\lambda)\sin\lambda t$$

For a case with $\omega_2(0) = \omega_3(0) = 0$, Eqs. (20c) and (20d) become

$$\dot{\theta}_2 = a/\lambda\{\cos(J_1/J)\Omega t - \cos\Omega t\} \tag{21a}$$

$$\dot{\theta}_3 = a/\lambda\{\sin(J_1/J)\Omega t - \sin\Omega t\} \tag{21b}$$

Integrating these equations with respect to time for the initial conditions of $\theta_2(0) = \theta_3(0) = 0$, we obtain

$$\theta_2 = A_p \sin\omega_p t - A_n \sin\omega_n t \tag{22a}$$

$$\theta_3 = A_p(1 - \cos\omega_p t) - A_n(1 - \cos\omega_n t) \tag{22b}$$

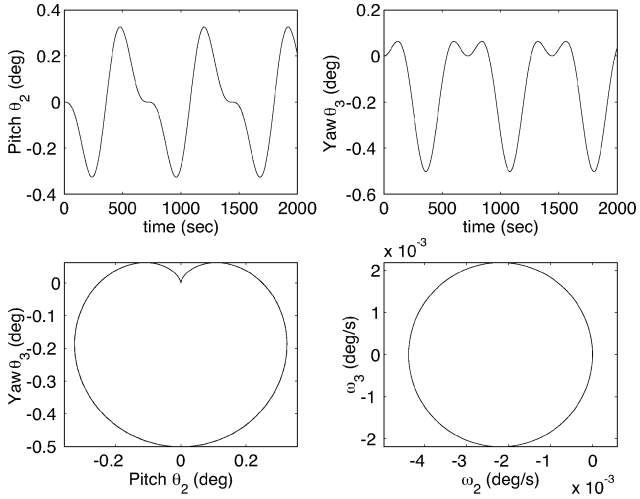

Fig. 8 Simulation results for a cm/cp offset of 0.1 m.

where

$$A_p = \frac{a}{\lambda\Omega}\frac{J}{J_1} = \text{precessional amplitude}$$

$$A_n = \frac{a}{\lambda\Omega} = \text{nutational amplitude}$$

$$\omega_p = \frac{J_1}{J}\Omega = \text{precessional frequency}$$

$$\omega_n = \Omega = \text{nutational frequency}$$

These equations can be used for preliminary dynamic analyses and/or tradeoffs for designing a spin-stabilized solar sail.

B. Example

The feasibility of spin-stabilizing a baseline 40×40 m sailcraft shown in Fig. 6, without employing a two-axis gimbaled control boom, is demonstrated here. For this sailcraft with an estimated cm/cp offset uncertainty of ± 0.1 m and a 0.01-N solar-pressure force, a spin rate of 0.5 deg/s is considered. The spin dynamics of this sailcraft is then characterized as

$$(J_1, J_2, J_3) = (6000, 3000, 3000)\ \text{kg} \cdot \text{m}^2$$

$$\frac{J_1}{J} = 2, \qquad \Omega = 0.5\ \text{deg/s}$$

$$\lambda = \frac{J_1 - J}{J}\Omega = 0.5\ \text{deg/s}$$

$$F = 0.01\ \text{N}, \qquad \epsilon = 0.1\ \text{m}$$

$$a = \frac{\epsilon F}{J} = 3.3 \times 10^{-7}\ \text{rad/s}^2$$

For these parameters, we obtain the precessional and nutation amplitudes as $A_p = 0.1254$ deg and $A_n = 0.2508$ deg. Therefore, it can be concluded that a low spin rate of 0.1–0.5 deg/s can keep the thrust-vector pointing error well within ± 1 deg for this sailcraft with a 0.1-m cm/cp offset and a 0.01-N solar pressure force. The simulation results are shown in Fig. 8. The plot of θ_3 vs θ_2 shows the path of the tip of the roll axis in space. However, high-fidelity dynamic modeling of a spinning sail will be needed to validate the simplified model used here, if such a spin-stabilization approach is actually to be employed for near-term solar sails.

V. Sailcraft in an Earth-Centered Elliptic Orbit

The Cosmos-1 solar sail mission of the Planetary Society may become the first experimental flight mission for solar sailing in an Earth-centered orbit. NASA, as well as Team Encounter and NOAA, is also planning to conduct solar sail validation flights in Earth-centered orbits. Although most future solar sails will be flying in sun-centered orbits, a variety of solar sail application missions in Earth-centered orbits are also being studied by NASA and DoD.

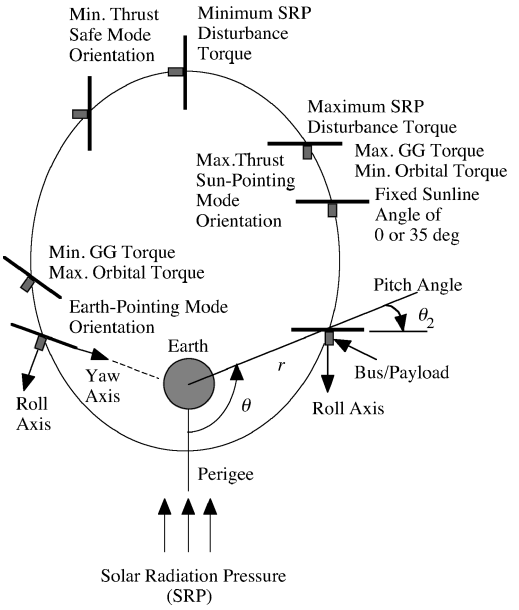

Fig. 9 Illustration of various pitch-control modes for a sailcraft in elliptic orbit.

This section provides a self-contained formulation of attitude dynamics of a solar sail in an Earth-centered elliptic orbit for the purpose of attitude-control analysis and design. Various orientations of a sailcraft in an Earth-centered orbit are illustrated in Fig. 9.

A. Dynamical Equations of Motion

Consider a sailcraft in an Earth-centered elliptic orbit. A local vertical and local horizontal (LVLH) reference frame A with its origin at the center of mass of an orbiting sailcraft has a set of unit vectors $\{\boldsymbol{a}_1, \boldsymbol{a}_2, \boldsymbol{a}_3\}$ with $\boldsymbol{a}_3$ locally vertical toward the Earth, $\boldsymbol{a}_1$ along the locally horizontal (transverse) direction, and $\boldsymbol{a}_2$ perpendicular to the orbit plane.

The angular velocity of such an LVLH reference frame A with respect to the earth-centered-inertial (ECI) reference frame is given by

$$\boldsymbol{\omega}^{A/E} = -\dot{\theta}\boldsymbol{a}_2 \tag{23}$$

where $\dot{\theta}$ is the orbital rate and θ is the true anomaly (satellite angular position) as measured from the perigee. The angular velocity of the body-fixed reference frame B with basis vectors $\{\boldsymbol{b}_1, \boldsymbol{b}_2, \boldsymbol{b}_3\}$ is then given by

$$\boldsymbol{\omega}^{B/E} = \boldsymbol{\omega}^{B/A} + \boldsymbol{\omega}^{A/E} = \boldsymbol{\omega}^{B/A} - \dot{\theta}\boldsymbol{a}_2 \tag{24}$$

where $\boldsymbol{\omega}^{B/A}$ is the angular velocity of B relative to A.

To describe the orientation of the body-fixed reference frame B with respect to the LVLH reference frame A in terms of three Euler angles $\theta_i (i = 1, 2, 3)$, consider the sequence of $\boldsymbol{C}_1(\theta_1) \leftarrow \boldsymbol{C}_3(\theta_3) \leftarrow \boldsymbol{C}_2(\theta_2)$ from the LVLH reference frame A to a body-fixed reference frame B. For this rotational sequence, we have

$$\begin{bmatrix} \boldsymbol{b}_1 \\ \boldsymbol{b}_2 \\ \boldsymbol{b}_3 \end{bmatrix} = \begin{bmatrix} C_{11} & C_{12} & C_{13} \\ C_{21} & C_{22} & C_{23} \\ C_{31} & C_{32} & C_{33} \end{bmatrix} \begin{bmatrix} \boldsymbol{a}_1 \\ \boldsymbol{a}_2 \\ \boldsymbol{a}_3 \end{bmatrix} \tag{25}$$

where C_{ij} are the direction cosine elements.

The rotational equation of motion of a rigid body with an angular momentum $\boldsymbol{H}$ is given by

$$\left\{\frac{d\boldsymbol{H}}{dt}\right\}_E \equiv \left\{\frac{d\boldsymbol{H}}{dt}\right\}_B + \boldsymbol{\omega}^{B/E} \times \boldsymbol{H} = \boldsymbol{M} \tag{26}$$

where $\{d/dt\}_E$ indicates differentiation with respect to time in reference frame E and $\{d/dt\}_B$ indicates differentiation with respect to time in reference frame B. The external torque vector, $\boldsymbol{M}$, is expressed as

$$\boldsymbol{M} = \frac{3\mu}{r^3}\boldsymbol{a}_3 \times \hat{J} \cdot \boldsymbol{a}_3 + \boldsymbol{u} \tag{27}$$

where $\boldsymbol{a}_3 \equiv -\boldsymbol{r}/r$, r is the radial distance of the sailcraft from the center of the Earth, $\hat{J}$ is the inertia dyadic of the sailcraft with respect to its mass center, and $\boldsymbol{u}$ is the control torque vector.

Because $\boldsymbol{H} = \hat{J} \cdot \boldsymbol{\omega}^{B/E}$, the attitude dynamical equations of motion can be rewritten as

$$\hat{J} \cdot \dot{\boldsymbol{\omega}} + \boldsymbol{\omega} \times \hat{J} \cdot \boldsymbol{\omega} = \frac{3\mu}{r^3}\boldsymbol{a}_3 \times \hat{J} \cdot \boldsymbol{a}_3 + \boldsymbol{u} \tag{28}$$

where $\boldsymbol{\omega} \equiv \boldsymbol{\omega}^{B/E}$ and $\dot{\boldsymbol{\omega}} = \{d\boldsymbol{\omega}/dt\}_E \equiv \{d\boldsymbol{\omega}/dt\}_B$. Expressing $\boldsymbol{\omega}, \boldsymbol{a}_3$, and $\hat{J}$ in terms of basis vectors of the body-fixed reference frame B as

$$\boldsymbol{\omega} = \omega_1\boldsymbol{b}_1 + \omega_2\boldsymbol{b}_2 + \omega_3\boldsymbol{b}_3 \tag{29a}$$

$$\boldsymbol{a}_3 = C_{13}\boldsymbol{b}_1 + C_{23}\boldsymbol{b}_2 + C_{33}\boldsymbol{b}_3 \tag{29b}$$

$$\hat{J} = \sum_{i=1}^{3}\sum_{j=1}^{3} J_{ij}\boldsymbol{b}_i\boldsymbol{b}_j \tag{29c}$$

we obtain the dynamical equations of motion about the body-fixed principal axes as

$$J_1\dot{\omega}_1 - (J_2 - J_3)\omega_2\omega_3 = -\frac{3\mu}{r^3}(J_2 - J_3)C_{23}C_{33} + u_1 \tag{30a}$$

$$J_2\dot{\omega}_2 - (J_3 - J_1)\omega_3\omega_1 = -\frac{3\mu}{r^3}(J_3 - J_1)C_{33}C_{13} + u_2 \tag{30b}$$

$$J_3\dot{\omega}_3 - (J_1 - J_2)\omega_1\omega_2 = -\frac{3\mu}{r^3}(J_1 - J_2)C_{13}C_{23} + u_3 \tag{30c}$$

where (u_1, u_2, u_3) are the control torque components along the body-fixed reference frame B and

$$C_{13} = -\sin\theta_2\cos\theta_3 \tag{31a}$$

$$C_{23} = \cos\theta_1\sin\theta_2\sin\theta_3 + \sin\theta_1\cos\theta_2 \tag{31b}$$

$$C_{33} = -\sin\theta_1\sin\theta_2\sin\theta_3 + \cos\theta_1\cos\theta_2 \tag{31c}$$

for the sequence of $\boldsymbol{C}_1(\theta_1) \leftarrow \boldsymbol{C}_3(\theta_3) \leftarrow \boldsymbol{C}_2(\theta_2)$ under consideration. For this rotational sequence we have the following kinematic differential equations:

$$\begin{bmatrix}\dot{\theta}_1\\ \dot{\theta}_2\\ \dot{\theta}_3\end{bmatrix} = \frac{1}{c\theta_3}\begin{bmatrix}c\theta_3 & -c\theta_1 s\theta_3 & s\theta_1 s\theta_3\\ 0 & c\theta_1 & -s\theta_1\\ 0 & s\theta_1 c\theta_3 & c\theta_1 c\theta_3\end{bmatrix}\begin{bmatrix}\omega_1\\ \omega_2\\ \omega_3\end{bmatrix} + \begin{bmatrix}0\\ \dot{\theta}\\ 0\end{bmatrix} \tag{32}$$

where $\dot{\theta}$ is the orbital rate, $c\theta_i \equiv \cos\theta_i$, and $s\theta_i \equiv \sin\theta_i$.

B. Earth-Pointing Sailcraft in an Earth-Centered Elliptic Orbit

In this section, the attitude equations of motion of a sailcraft which may need to be continuously pointing its yaw axis toward the Earth (i.e., edgewise toward the Earth) are derived. Such an "Earth-pointing" mode for minimizing the effect of gravity-gradient disturbance torque is illustrated in Fig. 9.

Assuming that θ_1 and θ_3 are small, θ_2 can be arbitrarily large, ω_1 and ω_3 are also small, and

$$\omega_1 \approx \dot{\theta}_1 - \dot{\theta}\theta_3 \tag{33a}$$

$$\omega_2 \approx \dot{\theta}_2 - \dot{\theta} \tag{33b}$$

$$\omega_3 \approx \dot{\theta}_3 + \dot{\theta}\theta_1 \tag{33c}$$

we obtain the attitude equations of motion as

$$J_1\ddot{\theta}_1 + \left(\dot{\theta}^2 + \frac{3\mu}{r^3}\cos^2\theta_2\right)(J_2 - J_3)\theta_1 - \dot{\theta}(J_1 - J_2 + J_3)\dot{\theta}_3 + \frac{3\mu}{r^3}(J_2 - J_3)(\sin\theta_2\cos\theta_2)\theta_3 = u_1 \tag{34a}$$

$$J_2\ddot{\theta}_2 + \frac{3\mu}{r^3}(J_1 - J_3)\sin\theta_2\cos\theta_2 = J_2\ddot{\theta} + u_2 \tag{34b}$$

$$J_3\ddot{\theta}_3 + (\dot{\theta}^2 + \frac{3\mu}{r^3}\sin^2\theta_2)(J_2 - J_1)\theta_3 + \dot{\theta}(J_1 - J_2 + J_3)\dot{\theta}_1 + \frac{3\mu}{r^3}(J_2 - J_1)(\sin\theta_2\cos\theta_2)\theta_1 = u_3 \tag{34c}$$

As can be seen in Eq. (34b), the pitch attitude equation has an orbital disturbance torque, $J_2\ddot{\theta}$, caused by the time-varying orbital rate $\dot{\theta}$.

Consider a sailcraft in an Earth-centered elliptic orbit with an eccentricity of e and a semimajor axis of a. Its orbital motion with slowly changing orbital elements is then described by

$$r = \frac{p}{1 + e\cos\theta} \tag{35}$$

where $p = a(1 - e^2)$, r is the radial distance of the sailcraft from the center of the Earth, and θ is the true anomaly. Furthermore, we have

$$\dot{r} = \sqrt{\frac{\mu}{p}}e\sin\theta \tag{36a}$$

$$\dot{\theta} = \sqrt{\frac{\mu}{p^3}}(1 + e\cos\theta)^2 \tag{36b}$$

$$\ddot{\theta} = \frac{2\mu}{p^3}(1 + e\cos\theta)^3 e\sin\theta \tag{36c}$$

where μ is the Earth's gravitational parameter. The orbital mean motion is defined as $n = \sqrt{(\mu/a^3)}$.

For small roll/pitch/yaw angles with respect to the LVLH frame, we obtain

$$J_1\ddot{\theta}_1 + \left(\dot{\theta}^2 + \frac{3\mu}{r^3}\right)(J_2 - J_3)\theta_1 - \dot{\theta}(J_1 - J_2 + J_3)\dot{\theta}_3 = u_1$$

$$J_2\ddot{\theta}_2 + \frac{3\mu}{r^3}(J_1 - J_3)\theta_2 = J_2\ddot{\theta} + u_2$$

$$J_3\ddot{\theta}_3 + \dot{\theta}^2(J_2 - J_1)\theta_3 + \dot{\theta}(J_1 - J_2 + J_3)\dot{\theta}_1 = u_3 \tag{37}$$

For a circular orbit with a constant orbital rate of $\dot{\theta} = n = \sqrt{\mu/a^3}$, we have

$$J_1\ddot{\theta}_1 + 4n^2(J_2 - J_3)\theta_1 - n(J_1 - J_2 + J_3)\dot{\theta}_3 = u_1$$

$$J_2\ddot{\theta}_2 + 3n^2(J_1 - J_3)\theta_2 = u_2$$

$$J_3\ddot{\theta}_3 + n^2(J_2 - J_1)\theta_3 + n(J_1 - J_2 + J_3)\dot{\theta}_1 = u_3 \tag{38}$$

which are the well-known linearized equations of motion of an Earth-pointing spacecraft in a circular orbit.

C. Sun-Pointing Sailcraft in an Earth-Centered Elliptic Orbit

The pitch axis of a "sun-pointing" sailcraft considered in this section is assumed to be perpendicular to the orbital plane (not to the ecliptic plane), as illustrated in Fig. 9. For such a sun-pointing sailcraft in an Earth-centered elliptic orbit with small body rates, $\omega_i (i = 1, 2, 3)$, and small roll/yaw angles, θ_1 and θ_3, the kinematic differential equations, (32), can be approximated as

$$\omega_1 \approx \dot{\theta}_1 \tag{39a}$$

$$\omega_2 \approx \dot{\theta}_2 - \dot{\theta} \tag{39b}$$

$$\omega_3 \approx \dot{\theta}_3 \tag{39c}$$

The attitude equations of motion with small roll and yaw angles in an Earth-centered elliptic orbit can then be obtained as

$$J_1\ddot{\theta}_1 + (\dot{\theta}^2 + \frac{3\mu}{r^3}\cos^2\theta_2)(J_2 - J_3)\theta_1 + \frac{3\mu}{r^3}(J_2 - J_3)(\sin\theta_2 \cos\theta_2)\theta_3 = u_1 \tag{40a}$$

$$J_2\ddot{\theta}_2 + \frac{3\mu}{r^3}(J_1 - J_3)\sin\theta_2 \cos\theta_2 = J_2\ddot{\theta} + u_2 \tag{40b}$$

$$J_3\ddot{\theta}_3 + \left(\dot{\theta}^2 + \frac{3\mu}{r^3}\sin^2\theta_2\right)(J_2 - J_1)\theta_3 + \frac{3\mu}{r^3}(J_2 - J_1)(\sin\theta_2 \cos\theta_2)\theta_1 = u_3 \tag{40c}$$

The pitch angle relative to the LVLH frame, θ_2, can be expressed as

$$\theta_2 = \theta - \frac{\pi}{2} + \alpha \tag{41}$$

where α is the sun angle between the surface normal and the sunline. In Fig. 9, the pitch angle θ_2 and the true anomaly θ are shown for an ideal case of $\alpha = 0$.

The pitch equation of motion of a sun-pointing sailcraft in terms of its sun angle α then becomes

$$J_2\ddot{\alpha} - \frac{3\mu}{r^3}(J_1 - J_3)\sin(\alpha - \theta)\cos(\alpha - \theta) = u_2 \tag{42}$$

D. Attitude Control of a Sailcraft Using Reaction Wheels

The feasibility as well as the limitations of employing a typical attitude control subsystem, which is often a necessary part of the sailcraft bus, is discussed here. Various pitch-control modes for an experimental sailcraft in an elliptic orbit, investigated for the NMP ST7 mission study, are illustrated in Fig. 9. Preliminary pitch-control analyses and simulation results are discussed here to emphasize the significant effects of the coupled attitude and orbital dynamics and the solar-pressure disturbance torque on sail-attitude control using reaction wheels.

The Earth-pointing pitch model of a sailcraft in an Earth-centered elliptic orbit is given by

$$J_2\ddot{\theta}_2 + \frac{3\mu}{r^3}(J_1 - J_3)\sin\theta_2 \cos\theta_2 = J_2\ddot{\theta} + u_2 + d_2 \tag{43}$$

where u_2 is the pitch-control torque and d_2 is the solar-pressure disturbance torque. The pitch equation (43) is often transformed to a dynamic model of the form

$$(1 + e\cos\theta)\theta_2'' - (2e\sin\theta)\theta_2' + \frac{3(J_1 - J_3)}{J_2}\sin\theta_2 \cos\theta_2 = 2e\sin\theta + \frac{(1+e)^3}{J_2(1 + e\cos\theta)^3}(u_2 + d_2) \tag{44}$$

where $(\,)' \equiv \mathrm{d}(\,)/\mathrm{d}\theta$. This model has been investigated extensively in the literature analyzing the effect of the periodic pitching excitation, $2e\sin\theta$, on the pitch-attitude motion of a rigid spacecraft in an elliptic orbit.

The sun-pointing pitch model of a sailcraft in an Earth-centered elliptic orbit is also given by

$$J_2\ddot{\alpha} - \frac{3\mu}{r^3}(J_1 - J_3)\sin(\alpha - \theta)\cos(\alpha - \theta) = u_2 + d_2 \tag{45}$$

where α is the sun angle related to θ and θ_2 as $\alpha = \theta_2 - \theta + \pi/2$.

For the purpose of studying the feasibility of stabilizing a sailcraft using a conventional attitude control system employing reaction wheels, we consider a simple model of reaction-wheel dynamics of the form

$$\dot{h}_2 = -u_2 \tag{46}$$

where h_2 is the pitch-wheel angular momentum. The solar-pressure disturbance torque caused by a cm/cp offset is also assumed to be

$$d_2 = \epsilon F \cos^2\alpha \cos^2 i \tag{47}$$

where F is the nominal solar-pressure force, ϵ is the cm/cp offset, and i is the orbital inclination angle from the ecliptic plane. Note that the nominal pitch axis is assumed to be perpendicular to the orbital plane and that small roll/yaw attitude angles are assumed.

For the baseline 40×40 m sailcraft, we assume that $F = 0.01$ N, $\epsilon = \pm 0.1$ m, and $(J_1, J_2, J_3) = (6000, 3000, 3000)$ kg $\cdot$ m^2. An Earth-centered elliptic orbit, called the supersynchronous transfer orbit (SSTO), chosen for a sail validation mission is characterized by

$$r_p = 6374 + 2000 = 8{,}374 \text{ km}$$

$$r_a = 6374 + 78{,}108 = 84{,}482 \text{ km}$$

$$a = (r_p + r_a)/2 = 46{,}428 \text{ km}$$

$$e = \frac{r_a - r_p}{r_a + r_p} = 0.8196$$

$$i = 12 \text{ deg (from the ecliptic plane)}$$

$$p = a(1 - e^2) = 15{,}238 \text{ km}$$

$$n = \sqrt{\frac{\mu}{a^3}} = 6.311 \times 10^{-5} \text{ rad/s}$$

and the orbital period of 27.65 h.

Pitch-control logic of the Earth-pointing mode is assumed to be

$$u_2 = -K_P\theta_2 - K_D\dot{\theta}_2 \tag{48}$$

and pitch-control logic of the sun-pointing mode to be

$$u_2 = -K_P(\alpha - \alpha_c) - K_D\dot{\alpha} \tag{49}$$

where α_c is the commanded sun angle. Controller gains of $K_P = 0.0865$ N $\cdot$ m/rad and $K_D = 22.78$ N-m/rad/s were selected for the closed-loop eigenvalues of $-0.005 \pm 0.005j$ rad/s.

Simulation results of flight-validating a sailcraft during continuous Earth-pointing-mode operation are shown in Fig. 10 for two consecutive orbits. The significant effect of the orbital disturbance torque, $J_2\ddot{\theta}$, on the pitch-wheel momentum requirement of a peak value of about 3.3 N $\cdot$ m $\cdot$ s can be seen in Fig. 10. The cm/cp offset was not included in this simulation.

Simulation results of continuous Earth-pointing-mode operation, including a cm/cp offset of 0.1 m, indicate that the sailcraft in an Earth-pointing mode may require a pitch wheel of momentum storage capability ± 15 N $\cdot$ m $\cdot$ s to counter both the solar-pressure and orbital-disturbance torques.

However, continuous sun-pointing mode operation of the 40-m sailcraft with a desired fixed sun angle of $\alpha = 35$ deg causes reaction-wheel momentum growth of about 100 N-m-s per orbit countering

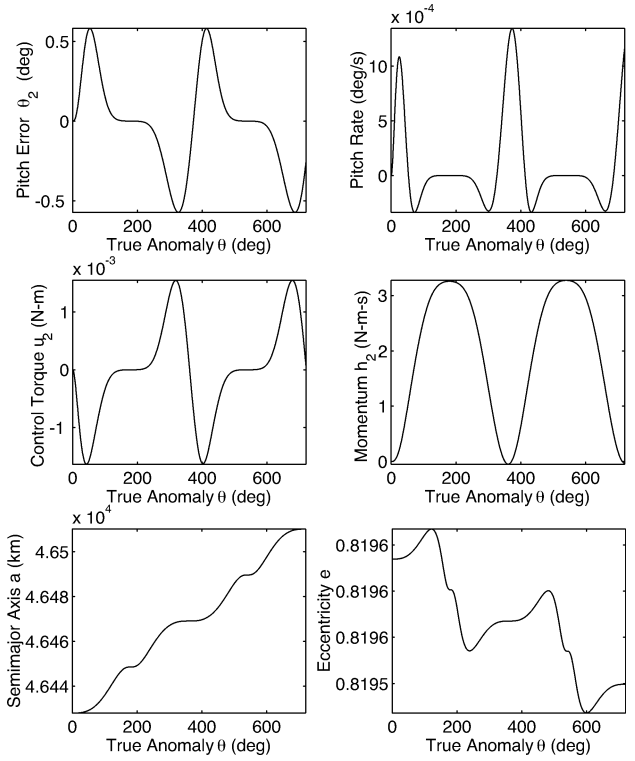

Fig. 10 Simulation results for the Earth-pointing mode, not including a cm/cp offset of 0.1 m.

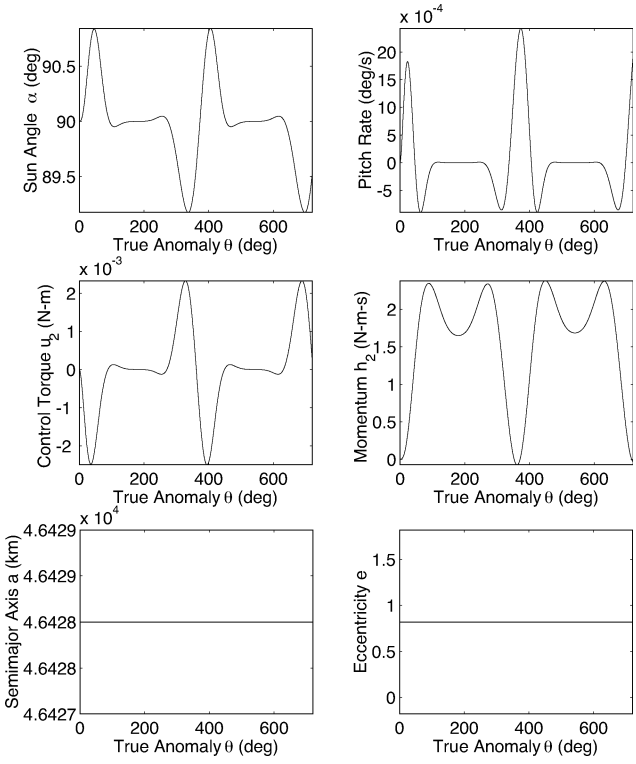

Fig. 11 Simulation results for the zero-thrust mode (desired sun angle α = 90 deg), including a cm/cp offset of 0.1 m.

a cm/cp offset of 0.1 m. Such momentum growth is excessive. Consequently, either spin stabilization or a cm/cp method needs to be employed for a sun-pointing sailcraft. The net change of the semimajor axis during each orbit is zero for such continuous sun-pointing mode operation with a fixed sun angle. With such a fixed sun angle, the semimajor axis increases when the sail is moving away from the sun, but it decreases when the sail is moving sunward. To increase the orbital energy or the semimajor axis, the sail needs to be oriented edgewise toward the sun when the sailcraft is moving sunward. Such a simple orbit-raising sail-steering profile requires two rapid 90-deg pitch maneuvers twice per orbit.

Simulation results for the baseline 40-m sailcraft in a zero-thrust mode are shown in Fig. 11. Although the effect of the solar-pressure disturbance torque is not significant because the edge of the sail is oriented toward the sun, the effect of the gravity-gradient torque on the pitch-wheel momentum storage requirement of about 2.5 N · m · s is also evident for this case.

In summary, a solar-pressure disturbance torque of 1 mN · m of the 40-m sailcraft when it is nominally sun pointing is about 100 times larger than that of typical geosynchronous communications satellites. Consequently, a nominally sun-pointing sailcraft in an Earth-centered orbit will need to be either spin-stabilized or three-axis-stabilized using control vanes or a gimbaled control boom.

E. Spin Stabilization of a Sailcraft in Earth-Centered Elliptic Orbit

A spin-stabilized, sun-pointing mode of a solar sail in an Earth-centered elliptic orbit is illustrated in Fig. 12. As derived in Sec. V.A the attitude dynamical equations of motion of such a spinning sailcraft in an Earth-centered elliptic orbit can be summarized as

$$J_1\dot{\omega}_1 - (J_2 - J_3)\omega_2\omega_3 = -\frac{3\mu}{r^3}(J_2 - J_3)C_{23}C_{33} \qquad (50a)$$

$$J_2\dot{\omega}_2 - (J_3 - J_1)\omega_3\omega_1 = -\frac{3\mu}{r^3}(J_3 - J_1)C_{33}C_{13} + \epsilon F \qquad (50b)$$

$$J_3\dot{\omega}_3 - (J_1 - J_2)\omega_1\omega_2 = -\frac{3\mu}{r^3}(J_1 - J_2)C_{13}C_{23} + \epsilon F \qquad (50c)$$

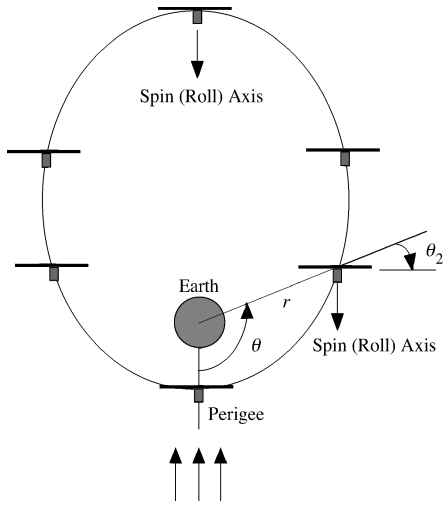

Fig. 12 Illustration of a spin-stabilized, sun-pointing mode for the sailcraft in elliptic orbit.

$$\begin{bmatrix}\dot{\theta}_1\\ \dot{\theta}_2\\ \dot{\theta}_3\end{bmatrix} = \frac{1}{c\theta_3}\begin{bmatrix}c\theta_3 & -c\theta_1 s\theta_3 & s\theta_1 s\theta_3\\ 0 & c\theta_1 & -s\theta_1\\ 0 & s\theta_1 c\theta_3 & c\theta_1 c\theta_3\end{bmatrix}\begin{bmatrix}\omega_1\\ \omega_2\\ \omega_3\end{bmatrix} + \begin{bmatrix}0\\ \dot{\theta}\\ 0\end{bmatrix} \qquad (51)$$

where $\dot{\theta}$ is the time-varying orbital rate, $c\theta_i \equiv \cos\theta_i$, $s\theta_i \equiv \sin\theta_i$, and the direction cosine elements, C_{ij}, are given by Eq. (31). The solar pressure disturbance torque is simply assumed as ϵF for both the pitch and yaw axes.

For the baseline 40 × 40 m sailcraft in a supersynchronous transfer orbit, nominal spin-mode conditions are assumed to be a spin rate of $\omega_1 = 0.5$ deg/s about the roll axis (as discussed in Sec. IV.B), a solar-pressure force of 0.01 N, a cm/cp offset of 0.1 m, and a nominal sun angle of 0 deg. Figure 13 shows two consecutive orbit simulation results of this nominal sun-pointing spin mode. The sun angle, $\alpha = \theta_2 - \theta + \pi/2$, is used as a pitch pointing error, and

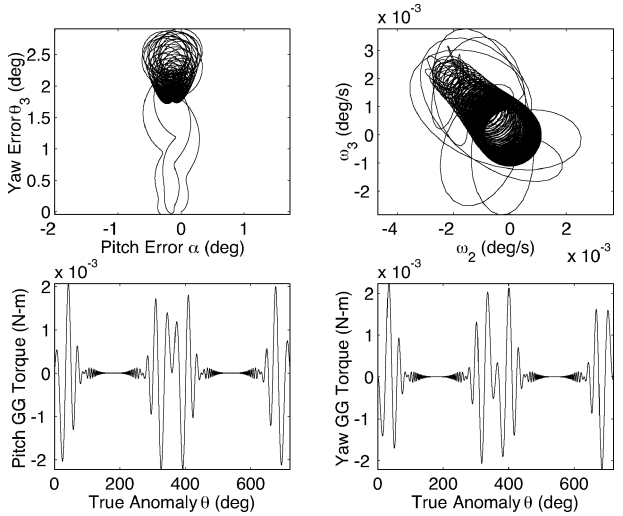

Fig. 13 Spin-mode simulation with a cm/cp offset of 0.1 m.

the gravity-gradient torques are expressed along the pitch/yaw axes fixed to the spinning sailcraft. The plot of θ_3 vs α shows the path of the tip of the roll axis in space. It can be seen that the gravity-gradient torques have caused a sun-pointing error of about 3 deg. The complex, but cyclic, nature of the gravity-gradient torques on a spinning sail in an Earth-centered elliptic orbit is evident here.

High-fidelity dynamic modeling of a spinning sail will be needed to validate the simplified model used here, if such a spin-stabilization approach is actually to be employed for near-term solar sails.

VI. Conclusions

Dynamical modeling and analysis of a sailcraft in an Earth-centered elliptic orbit have been presented, with particular emphasis on the significant effect of a solar-pressure disturbance torque (caused by an uncertain center-of-mass and center-of-pressure offset) on sailcraft attitude stability and pointing. A 40×40 m, 160-kg sailcraft with a nominal solar pressure force of 0.01 N, an uncertain cm/cp offset of ± 0.1 m, and moments of inertia of (6000, 3000, 3000) $\text{kg} \cdot \text{m}^2$ was used to illustrate the various concepts and principles involved in dynamic modeling and attitude control design. The study results will provide sail mission designers with options and approaches to meet the various requirements of near-term sails as well as future advanced solar sails.

Acknowledgments

This research has been supported by JPL Contract 1228156 from the Solar Sail Technology Working Group of the NASA In-Space Propulsion Program. It was also in part supported by the New Millennium Program Space Technology 7 Solar Sail Concept Study Project. The author thanks H. Price at the Jet Propulsion Laboratory, L. Johnson at NASA Marshall Space Flight Center, and C. Moore at NASA Langley Research Center for their supporting this research. The various solar-sail control concepts described in this paper are currently being further investigated for a solar sail ground validation experiment of the NASA In-Space Propulsion program, managed by G. Garbe and E. Montgomery at NASA MSFC. The author also thanks the reviewers and the Associate Editor, Panagiotis Tsiotras, for their comments and suggestions, which significantly improved the quality of this paper.

References

[1]Price, H., Ayon, J., Buehler, M., Garner, C., Klose, G., Mettler, E., Nakazono, B., and Sprague, G., "Design for a Solar Sail Demonstration Mission," Space Technology and Applications International Forum (STAIF 2001), Albuquerque, NM, Feb. 2001.

[2]West, J. L., and Derbes, B., "Solar Sail Vehicle System Design for the Geostorm Warning Mission," AIAA Paper 2000-5326, Sept. 2000.

[3]Rogan, J., Gloyer, P., Pedlikin, J., Veal, G., and Derbes, B., "Encounter 2001: Sailing to the Stars," Paper SSC01-II-2, Utah State University, Logan, UT, Aug. 2001.

[4]Cohen, D., Gloyer, P., and Rogan, J., "Preliminary Design of a High Performance Solar Sailing Mission," Paper SSC02-II-5, Utah State University, Logan, UT, Aug. 2002.

[5]Murphy, D. M., Murphey, T. W., and Gierow, P. A., "Scalable Solar Sail Subsystem Design Considerations," AIAA 2002-1703, April 2002.

[6]Wright, J. L., *Space Sailing*, Gordon and Breach, New York, 1992.

[7]Friedman, L., *Star Sailing: Solar Sails and Interstellar Travel*, Wiley, New York, 1988.

[8]McInnes, C. R., *Solar Sailing: Technology, Dynamics and Mission Applications*, Springer Praxis, 1999.

[9]Garwin, R. L., "Solar Sailing–A Practical Method of Propulsion Within the Solar System," *Jet Propulsion*, Vol. 28, No. 3, 1958, pp. 188–190.

[10]Sohn, R. L., "Attitude Stabilization by Means of Solar Radiation Pressure," *ARS Journal*, Vol. 29, May 1959, pp. 371–373.

[11]Acord, J. D., and Nicklas, J. C., "Theoretical and Practical Aspects of Solar Pressure Attitude Control for Interplanetary Spacecraft," *Guidance and Control II*, Progress in Astronautics and Aeronautics, Vol. 13, Academic Press, New York, 1964, pp. 73–101.

[12]Modi, V. J., and Kumar, K., "Attitude Control of Satellites Using the Solar Radiation Pressure," *Journal of Spacecraft and Rockets*, Vol. 9, No. 9, 1972, pp. 711–713.

[13]Joshi, V. K., and Kumar, K., "New Solar Attitude Control Approach for Satellites in Elliptic Orbits," *Journal of Guidance and Control*, Vol. 3, No. 1, 1980, pp. 42–47.

[14]Stuck, B. W., "Solar Pressure Three-Axis Attitude Control," *Journal of Guidance and Control*, Vol. 3, No. 2, 1980, pp. 132–139.

[15]Angrilli, F., and Bortolami, S., "Attitude and Orbital Modelling of Solar-Sail Spacecraft," *European Space Agency Journal*, Vol. 14, No. 4, 1990, pp. 431–446.

[16]Renner, U., "Attitude Control by Solar Sailing: A Promising Experiment with OTS-2," *European Space Agency Journal*, Vol. 3, No. 1, 1979, pp. 35–40.

[17]Lievre, J., "Solar Sailing Attitude Control of Large Geostationary Satellite," *IFAC Automatic Control in Space*, Pergamon, Oxford, 1985, pp. 29–33.

[18]Azor, R., "Solar Attitude Control Including Active Nutation Damping in a Fixed-Momentum Wheel Satellite," *Proceedings of AIAA Guidance, Navigation, and Control Conference*, AIAA, Washington, DC, Aug. 1992, pp. 226–235.

[19]Sidi, M. J., *Spacecraft Dynamics and Control: A Practical Engineering Approach*, Cambridge Univ. Press, Cambridge, England, U.K., 1997, pp. 229–236.

[20]Burns, R., Gabor, M. J., McLaughlin, C. A., Luu, K. K., and Sabol, C., "Solar Radiation Pressure Effects on Formation Flying of Satellites with Different Area-to-Mass Ratios," AIAA Paper 2000-4132, Aug. 2000.

[21]Williams, T., and Wang, Z.-S., "Potential Non-Propulsive Stationkeeping Techniques for Picosatellite Formation Flight," AIAA Paper 2000-4134, Aug. 2000.

[22]Wie, B., and Roithmayr, C., "Integrated Orbit, Attitude, and Structural Control Systems Design for Space Solar Power Satellites (SSPS)," AIAA Paper 2001-4273, Aug. 2001; also NASA TM-2001-210854, June 2001.

[23]Bryson, A. E., Jr., *Control of Spacecraft and Aircraft,* Princeton Univ. Press, Princeton, NJ, 1994, Chaps. 5–10.

[24]Wie, B., *Space Vehicle Dynamics and Control*, AIAA Education Series, AIAA, Reston, VA, 1998, Chaps. 7 and 9.

[25]Wie, B., "Solar Sail Attitude Control and Dynamics, Part 2," *Journal of Guidance, Control, and Dynamics*, Vol. 27, No. 4, pp. 536–544.

[26]Agrawal, B. N., *Design of Geosynchronous Spacecraft*, Prentice–Hall, Upper Saddle River, NJ, 1986, pp. 133–135.